The Astrophysical Journal, 702:1016–1024, 2009 September 10 doi:10.1088/0004-637X/702/2/1016

ESTIMATING THE CHROMOSPHERIC ABSORPTION OF TRANSITION REGION MOSS EMISSION

Bart De Pontieu[1], Viggo H. Hansteen[1,2], Scott W. McIntosh[3], and Spiros Patsourakos[4,5]
[1] Lockheed Martin Solar and Astrophysics Lab, 3251 Hanover Street, Org. ADBS, Bldg. 252, Palo Alto, CA 94304, USA; bdp@lmsal.com
[2] Institute of Theoretical Astrophysics, University of Oslo, Blindern, Oslo 315, Norway
[3] High Altitude Observatory, National Center for Atmospheric Research, P.O. Box 3000, Boulder, CO 80307, USA
[4] Naval Research Laboratory, Space Science Division, Washington, DC 20375, USA
[5] Center for Earth Observing and Space Research, George Mason University, Fairfax, VA 22030, USA
Received 2009 March 24; accepted 2009 July 13; published 2009 August 18

ABSTRACT

Many models for coronal loops have difficulty explaining the observed EUV brightness of the transition region, which is often significantly less than theoretical models predict. This discrepancy has been addressed by a variety of approaches including filling factors and time-dependent heating, with varying degrees of success. Here, we focus on an effect that has been ignored so far: the absorption of EUV light with wavelengths below 912 Å by the resonance continua of neutral hydrogen and helium. Such absorption is expected to occur in the low-lying transition region of hot, active region loops that is colocated with cool chromospheric features and called "moss" as a result of the reticulated appearance resulting from the absorption. We use cotemporal and cospatial spectroheliograms obtained with the *Solar and Heliospheric Observatory*/SUMER and *Hinode*/EIS of Fe XII 1242 Å, 195 Å, and 186.88 Å, and compare the density determination from the 186/195 Å line ratio to that resulting from the 195/1242 Å line ratio. We find that while coronal loops have compatible density values from these two line pairs, upper transition region moss has conflicting density determinations. This discrepancy can be resolved by taking into account significant absorption of 195 Å emission caused by the chromospheric inclusions in the moss. We find that the amount of absorption is generally of the order of a factor of 2. We compare to numerical models and show that the observed effect is well reproduced by three-dimensional radiative MHD models of the transition region and corona. We use *STEREO A*/*B* data of the same active region and find that increased angles between line of sight and local vertical cause additional absorption. Our determination of the amount of chromospheric absorption of TR emission can be used to better constrain coronal heating models.

Key words: Sun: atmospheric motions – Sun: chromosphere – Sun: corona – Sun: magnetic fields – Sun: transition region

Online-only material: color figures

1. INTRODUCTION

The nature of the transition region continues to be the subject of significant debate. As part of the interface between the photosphere and corona, it plays an important role in the transport and deposition of the nonthermal energy believed to power the heating of both chromosphere and corona. It is now well established that the interface between the photosphere and corona does not resemble the view suggested by hydrostatic, spherically symmetrical, and time-averaged models. Instead, the chromosphere is a highly dynamic environment (Rutten 2006) with jets, such as fibrils, spicules, and mottles (Hansteen et al. 2006; De Pontieu et al. 2007a, 2007b; Rouppe van der Voort et al. 2007) continuously perturbing the thermodynamic quantities and density stratification from their equilibrium values. As a result of these significant deviations from hydrostatic equilibrium, the transition region is molded by the same dynamic spicular features as the chromosphere. There is ample evidence that between a height range of roughly 2000 and 10,000 km above the photosphere, plasma with temperatures ranging from 10,000 K to 1 MK co-exist and "mingle" in a highly dynamic fashion. However, the availability of time-averaged, one-dimensional models of the chromosphere and transition region has allowed coronal loop models to ignore the complexities and inherently dynamic nature of this interface (for a review, see Klimchuk 2006). Neglecting the intricacies of the chromosphere can be problematic since the chromospheric heating mechanism requires 50 times more energy than the coronal heating mechanism. Consequently, it is perhaps not surprising that a full explanation of coronal heating remains outstanding, with many unresolved issues and problems (but see Aschwanden et al. 2007, for a different approach).

One of these issues that has been problematic for theoretical models of coronal loops is the large discrepancy between the observed and predicted emission from the transition region in coronal loops. A variety of theoretical models predicts emission in transition region lines much in excess of what is observed with EUV imagers such as the *Solar and Heliospheric Observatory* (*SOHO*)/EUV Imaging Telescope and the *Transition Region and Coronal Explorer* (*TRACE*). This manifests itself in large differences in predicted brightness between active region loops and transition region moss. Moss is low-lying, strong EUV emission that was discovered in *TRACE* EUV images in the Fe IX/X 171 Å and Fe XII 195 Å passbands (Berger et al. 1999a, 1999b; De Pontieu et al. 1999; Fletcher & De Pontieu 1999). It is the upper transition region at the base of hot, high-pressure loops (Berger et al. 1999b; Martens et al. 2000). Observations show that in a typical Fe IX/X 171 Å EUV image of an active region, coronal loops and moss regions are roughly of the same brightness. Despite a variety of approaches, all theoretical models continue to predict much higher EUV emission from moss regions than from coronal loops. For example, most coronal loop models based on a steady heating mechanism predict moss emission that is one to several orders of magnitude

larger than what is observed (Schrijver et al. 2004; Warren & Winebarger 2006; Warren et al. 2008). While the introduction of models based on time-dependent nanoflare heating (e.g., Patsourakos & Klimchuk 2008) on average shows a smaller discrepancy, they still predict moss emission that is 10 times brighter than what is sometimes observed. Other models remove the discrepancy by introducing a filling factor in the transition region as a free parameter (Winebarger et al. 2008).

However, none of these models take into account the fact that the transition region emission in moss regions as observed by EUV imagers such as *TRACE* and EUV Imaging Telescope (EIT) undergoes significant absorption by neutral gas through Lyman continuum absorption. Radiation of EUV emission below the head of the hydrogen Lyman continuum at 912 Å can be absorbed by neutral hydrogen (Anzer & Heinzel 2005). In addition, neutral helium can absorb EUV radiation with wavelengths shorter than 504 Å and singly ionized helium can contribute to absorption for wavelengths shorter than 228 Å. The effects of neutral hydrogen and helium and singly ionized helium on EUV radiation were studied extensively in the past (Schmahl & Orrall 1979; Doschek & Feldman 1982; Mariska 1992; Daw et al. 1995; Judge et al. 1995; Anzer & Heinzel 2005) for a variety of solar regions including quiet Sun, coronal holes, prominences, the limb, and active regions, often with confusing results and interpretations. Part of this confusion likely stems from the fact that the amount of neutral plasma in observations of such a wide variety of features is highly variable and most often not directly observed, but simply inferred from the EUV emission. This is not the case for moss: high-resolution observations made in the EUV (with *TRACE*) and chromospheric lines such as Hα (with ground-based telescopes) clearly show the presence of neutral plasma at heights where EUV emission occurs (Berger et al. 1999b). In fact, moss shows up as a reticulated pattern above plage regions precisely because the EUV emission from the 1–1.5 MK upper transition region plasma is absorbed by mostly neutral gas in dense, chromospheric jets or fibrils that occur at similar heights and in the immediate surroundings of the upper transition region plasma (De Pontieu et al. 1999).

The mingling of chromospheric and TR plasma at low heights has been confirmed by several observational studies in the past few years. For example, De Pontieu et al. (2003b) found that in moss regions the linecenter intensity of one of the dominant chromospheric lines (Hα) is very well correlated, both spatially and temporally, with Fe IX/X EUV emission observed with *TRACE*. Such a correlation is difficult to understand unless chromospheric and TR plasma occur at similar heights. This is confirmed by De Pontieu et al. (2003a) who found that oscillations in moss, observed in EUV with *TRACE*, are associated with oscillations in the wings of Hα. These correlated oscillations can be explained by absorption of EUV emission by chromospheric fibrils that quasi-periodically rise high enough so that they can obscure the lower-lying upper TR emission from neighboring field lines (De Pontieu et al. 2004). Such a scenario is supported by extensive observational and modeling work that has shown that these dynamic fibrils are caused by shock waves that drive chromospheric plasma upward to reach heights of several 1000 km (De Pontieu et al. 2004, 2007a; De Pontieu & Erdélyi 2006; Hansteen et al. 2006; Heggland et al. 2007).

An accurate determination of this absorption in moss regions is thus clearly an important ingredient in determining the accuracy (or constraining parameters such as filling factors) of coronal loop models. In this paper, we focus on determining what fraction of the EUV emission in moss regions is absorbed, so that future work can directly compare predicted intensities with observed intensities that have been corrected for this absorption.

We use the density sensitivity of emission lines (of the same ion) formed above and below the Lyman continuum and compare the obtained densities from several line pairs. We describe the observations with *Hinode* (Kosugi et al. 2007) and *SOHO* (Domingo et al. 1995) and the co-alignment of the EIS (Culhane et al. 2007) and Solar Ultraviolet Measurement of Emitted Radiation (SUMER; Wilhelm et al. 1995) spectra in Section 2. In Section 3, we describe the discrepancies in density measurements for coronal loops and moss regions, and estimate the amount of absorption of TR emission. We also observe the same moss region with SECCHI (Howard et al. 2008) onboard the *STEREO A* and *B* spacecraft (Kaiser et al. 2008) and use the dependence on viewing angle of the TR emission to estimate the center-to-limb variation of the absorption (Section 4). We demonstrate that such absorption compares well with what we detect in numerical simulations (Section 5). We finish by summarizing our results and briefly discussing the potential impact of our results on coronal loop modeling in Section 6.

2. DETAILS OF EIS/SUMER OBSERVATIONS

To study the differential absorption of EUV emission with wavelengths below and above 912 Å, we focus on emission lines from the same ion that is formed, under ionization equilibrium conditions, at temperatures that are high enough to clearly show moss ($\log T = 5.7$–6.3). These conditions are quite stringent since most high-temperature lines above 912 Å are forbidden lines and quite weak. In addition, the small-scale nature of moss structuring requires 1″–2″ class spectra in both lines. The launch of *Hinode* and its EIS instrument has opened up access to a range of Fe XII lines (186.88 and 195.1 Å in particular) that together with SUMER's Fe XII 1242 Å line provide the tools we require to address the absorption of EUV moss emission by neutral hydrogen and helium (and singly ionized helium). We have chosen these lines because the 186.88 Å and 195.1 Å line pair is sensitive to densities in the range of $\log n_e = 8$–10.5, an ideal range for active regions. In addition, the ratio of 195 to 1242 Å is also sensitive to density, so that we can directly compare the densities derived from both line pairs.

We use an EIS raster of a weak active region (which lacks a NOAA number) taken from 16:44 to 17:50 UTC on 2007 November 14 (see panels (a) and (b) of Figure 1). The active region was observed at a heliocentric position of (+150″, −100″). The raster consists of spectra of a range of EUV emission lines (including Fe XII 186.88 and 195.1 Å) at 256 positions (spaced 1″ apart in solar x) observed from west to east at a cadence of 15 s. The data are despiked (i.e., cosmic ray removal) and calibrated using `eis_prep.pro` in the EIS solarsoft software tree. For each location in the raster, we calculate the total intensity in the Fe XII lines by summing over a range of spectral pixels that includes the full line, and subtracting an estimate of the continuum emission in a spectral region in the immediate spectral vicinity that is free of emission lines. The absolute calibration of EIS is described in Culhane et al. (2007) and is estimated to be accurate to about 20%. We remove the pointing offset between the EIS rasters by using a cross-correlation technique between the two Fe XII rasters.

During the same time frame SUMER observed this active region in a range of UV lines that include the Fe XII 1242 Å

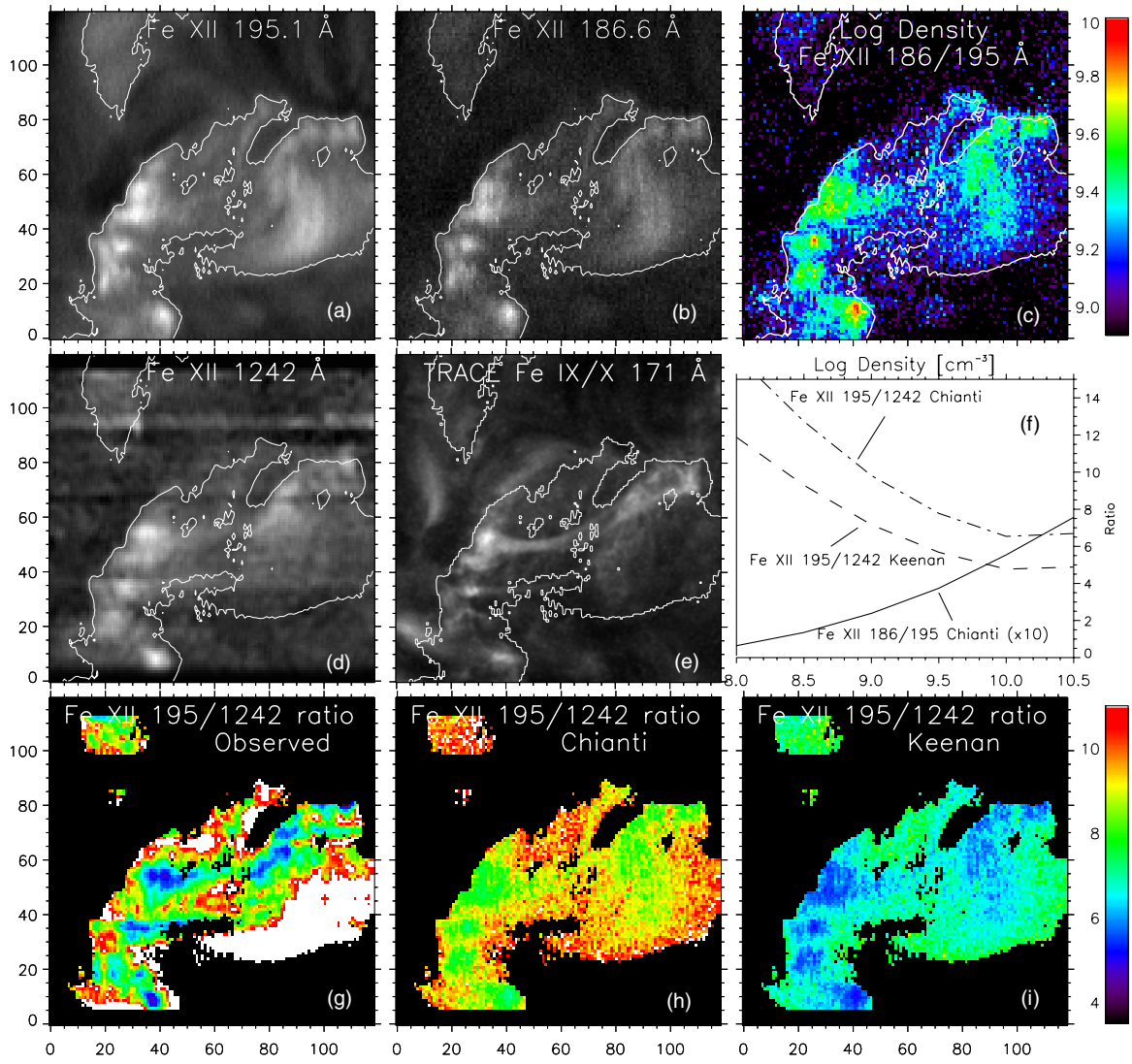

Figure 1. Top row shows a spectroheliogram in Fe XII 195.1 Å and 186.88 Å taken on 2007 November 14 from 16:44 to 17:50 UTC with EIS, as well as the logarithm of the density as determined from the line ratio of the 186.88 and 195.1 Å lines. The middle row shows the slightly spatially smoothed SUMER raster taken from 17:12 through 20:33 UT and a *TRACE* Fe IX/X 171 Å image. The middle right panel shows the line ratio to density functions we used to determine the density for both line pairs. The Fe XII 186/195 Å line ratio is multiplied by 10 for illustration purposes. The bottom row shows the observed Fe XII 195/1242 Å line ratio, as well as the line ratio that is predicted if we use the density determination of the 186/195 line ratio, for two atomic models: CHIANTI and that of Keenan et al. (1990). The overplotted contours correspond to a brightness threshold in the EIS Fe XII 195.1 Å raster. See the text for details on the interpretation.

(A color version of this figure is available in the online journal.)

emission line. Similarly to both EIS lines, it has a peak in the contribution function at $\log T = 6.15$. The raster was taken from east to west and took much longer to complete (from 17:12 UTC through 20:35 UTC) because of the different SUMER sensitivity and the weakness of the Fe XII line. The raster steps are 1.″125 with three exposures of 30 s at each raster position to ensure an adequate count rate. To calibrate the SUMER data we perform the steps described in McIntosh et al. (2007) which includes corrections for flat-fielding, as well as the absolute calibration. The last available flat-field is from 2001, which means that there are some uncertainties in correcting for detector artifacts. This is clearly visible in panel (d) of Figure 1 which shows the SUMER Fe XII 1242 Å intensity (calculated in the same way as described for EIS in the above). The uncertainty in flat-fielding is evidenced by the presence of bright and dark horizontal streaks in the raster.

To co-align these rasters we perform the following steps. Since these rasters have very different durations, they are subject to substantially different solar rotation effects with the features rastered by SUMER rotating by 30″, with EIS only undergoing 10″. To remove this effect, we recalculate the pointing information for each position of the EIS and SUMER rasters back to the same reference time t_0. In other words, we calculate which features on the Sun at t_0 occupy the SUMER and EIS slits at the diverse range of positions and times of the rasters. Using this new pointing information, we then calculate which SUMER raster positions are nearest in space to the EIS raster positions, and form a SUMER raster that has the same spatial scale and number of positions as the EIS rasters. As a final step we perform a final coalignment between the new SUMER raster and the EIS rasters through visual comparison of the features in the eastern half of the overlapping parts of the field of view. We focus on the eastern half because the time difference between the SUMER and EIS exposures in that area of the field of view are the smallest, of the order of ± 1 hr (see the bottom panel of Figure 3), which

increases the likelihood of viewing the same coronal and TR structures.

The resulting co-alignment, shown in Figure 1, is quite satisfactory, especially in the eastern half of the raster. We use simultaneous *TRACE* and XRT data to identify the locations of TR moss. The high spatial resolution of the *TRACE* Fe IX/X 171 Å image (formed at slightly lower temperatures of 1 MK, and taken around 17:45 UTC) shows the reticulated pattern that is typical for TR moss. This pattern is caused by the presence of EUV absorbing chromospheric features; typically jets or dynamic fibrils (De Pontieu et al. 2003a, 2003b, 2004, 2007a; Hansteen et al. 2006). We find several patches of moss around $x = 20$–40 and $y = 0$–70 (MA), as well as $x = 75$–120 and $y = 60$–90 (MB). Those footpoint locations fit very well with the location of the associated hotter loops in the two XRT images in Figure 3. In addition, comparison of the Fe XII rasters with the XRT images allows us to identify coronal loops in the Fe XII rasters around $x = 10$–40 and $y = 80$–120 (A), as well as $x = 60$–120 and $y = 30$–60 (B), and some smaller loops around $x = 10$–25 and $y = 0$–15 (C), $x = 20$ and $y = 25$–35 (D), $x = 60$–80 and $y = 65$–85 (E), and $x = 40$–65 and $y = 60$–75 (F).

The XRT images (Figure 3) are taken at roughly the beginning and end of the SUMER raster and show the significant changes the western half of the active region undergoes during the 3 hr raster. We draw attention to the formation of moss footpoints around $x = 80$–120 and $y = 60$–70 and associated loops just south of that region. These changes all occur after the EIS raster has ended. This explains the different appearance in panels (a), (b), and (d) of Figure 1 of the Fe XII emission in the southwestern part of the field of view. The eastern part of the active region shows much less variability with stable moss patterns. This is the region we will focus on in the following.

3. ANALYSIS OF EIS/SUMER OBSERVATIONS

We calculate the density sensitivity of the Fe XII 186.88 and 195.1 Å lines by using CHIANTI (Dere et al. 1997). The line ratio is sensitive to densities between $\log n_e = 8.5$ and 10.5, as shown in panel (f) of Figure 1. We calculate the intensities as described in Section 2, and then determine the ratio of the 186.88 Å and 195.1 Å intensity. We use the curve in panel (f) to calculate the density shown in panel (c) of Figure 1. We find densities of the order of 10^9 cm^{-3} in the coronal loops we have identified earlier, with significantly higher densities of the order of 4×10^9–10^{10} cm^{-3} in the moss regions. These values are very reasonable, and similar to those found in active region loops and moss regions reported by Fletcher & De Pontieu (1999) and Warren et al. (2008) using CDS and EIS, respectively.

We can use the densities determined from this line ratio to calculate what the intensity ratio between the 195 Å and 1242 Å lines should be, given the density sensitivity of the latter ratio. This density sensitivity is not as straightforward to use as the 186/195 ratio. First, there is some discussion regarding the atomic physics underlying the density sensitivity, with Keenan et al. (1990) and CHIANTI (Dere et al. 1997) giving slightly different curves of line ratio to density (see panel (f) of Figure 1), with the Keenan et al. (1990) results showing lower ratios by a factor of 0.73. In what follows we will use both and compare the results. Using the density derived from 186/195 Å and the CHIANTI and Keenan et al. (1990) curves, we now calculate for each position in the rasters the predicted Fe XII 195/1242 Å intensity ratio (shown in panels (h) and (i) of Figure 1).

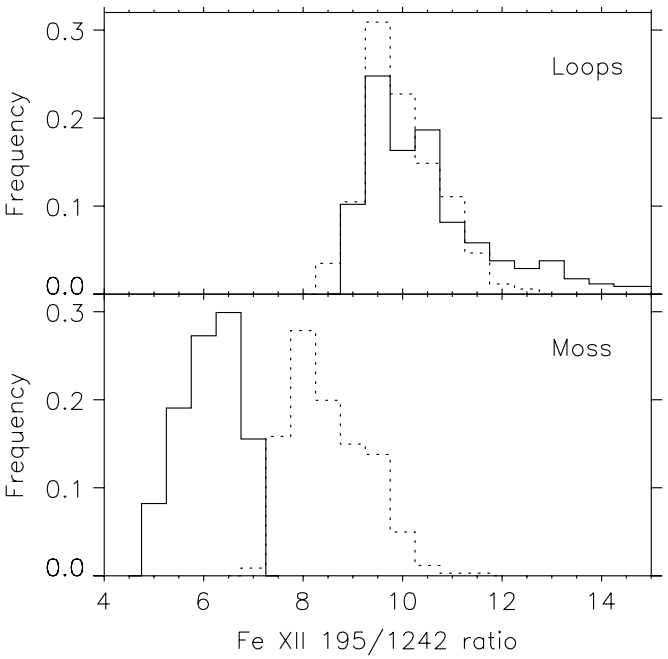

Figure 2. Comparison of histograms of the observed (full lines) and predicted (dotted lines) values of the 195.1 Å to 1242 Å intensity ratio in coronal loops A and F (top row), and moss region MA (bottom row). See Section 2 for the definition and location of loop and moss regions.

The values of this ratio vary between 8 and 12 for the CHIANTI curve, and between 5 and 8 for the Keenan et al. (1990) curve.

We now calculate the Fe XII 195/1242 Å ratio directly from the observations using the coaligned rasters. The Fe XII 1242 Å raster is quite noisy because of the low count rates, so we use a boxcar smoothing over 3 pixels to remove some of that noise when calculating the ratio between the EIS and SUMER rasters. The resulting ratio is shown in panel (g) of Figure 1 with the same color table as panels (h) and (i). The observed ratio varies between 5 and 15 and generally shows a much better correspondence with the levels predicted by the CHIANTI curve. However, it is immediately clear that there are also significant differences between the predicted and observed intensity ratios. The most striking difference is that the moss regions in the eastern half of the field of view systematically show lower ratios (of the order of 4–6) than predicted (of the order of 8 to 10). This implies that the EUV emission with wavelengths below 912 Å is weaker by a factor of the order 2 in moss regions than would be expected. In contrast the loop structures we identified in the above show a much better correspondence with typically values around 10 (yellow) in both the observed and predicted maps, especially for loops A, C, D, and E.

Figure 2 shows these differences in more detail by comparing histograms of the predicted and observed 195/1242 intensity ratio for coronal loops A and F (top panel), as well as moss region MA (bottom panel). As we can see, the loop regions show reasonable correspondence between the predicted and observed ratios, whereas the moss regions show a significant difference of the order of 2.

The loop regions often show higher observed values than predicted. This can be seen in Figure 2, but also in the large loops B in Figure 1. We believe this is likely because the active region thermal structure in the western half of the field of view changed toward the end of the SUMER raster, so that the Fe XII

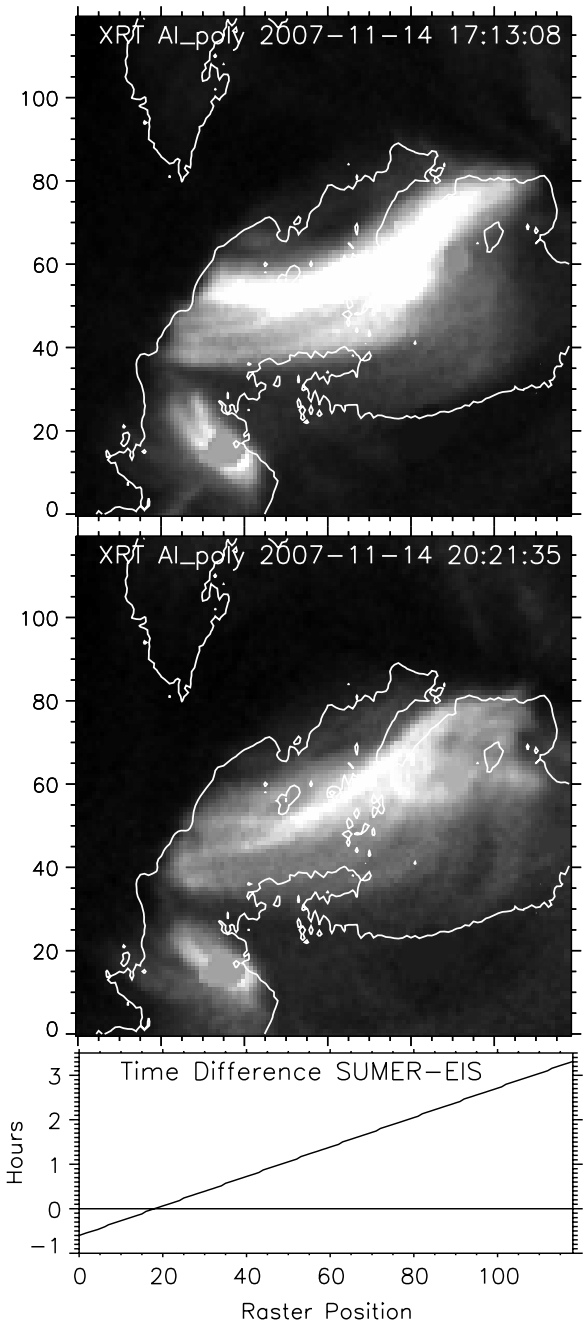

Figure 3. Top two images show XRT images (Al_{poly}) taken at the beginning and end of the SUMER raster. The overplotted contours again correspond to the same brightness threshold in the EIS Fe XII 195 Å raster shown in Figure 1. Since the XRT filter is sensitive to hotter plasma than the Fe XII rasters, we see much more emission from the hot loops connecting the TR moss footpoints. In addition, we see that the loop structure in the middle right of the image drastically changes in morphology with new moss footpoints appearing around $x = 80$–120, $y = 60$. The lower panel shows, in hours, the time difference between the SUMER and EIS exposures (shown in Figure 1) at each co-aligned raster location. The time differences are caused by the different durations of the SUMER and EIS rasters, and the fact that they raster in E–W and W–E directions, respectively. The left part of the rasters is taken within 1 hr of each other, whereas the right part ($x > 70$) shows exposures that are taken 2 or more hours apart. See the text for details.

1242 Å emission becomes much lower, perhaps because of a heating of the loops in that region toward the end of the SUMER raster (which is suggested by the XRT time series, Figure 3). In this scenario, the EIS raster, taken 3 hr earlier then still shows evidence of the cooler loops.

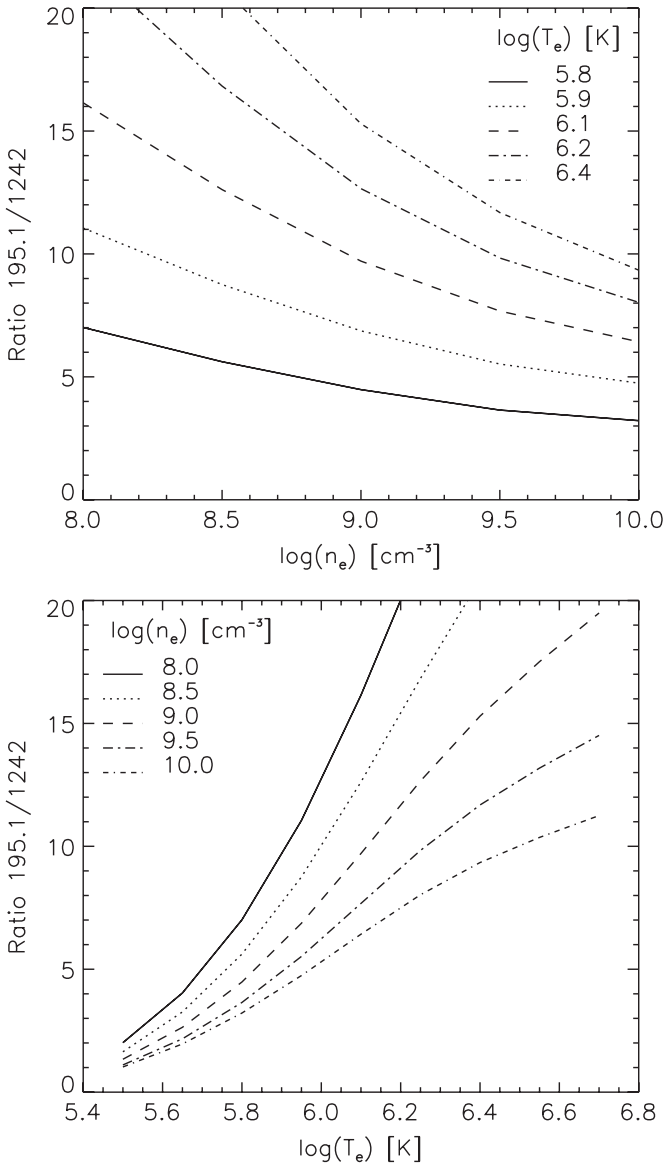

Figure 4. Density sensitive intensity ratio of the Fe XII 195 Å and 1242 Å lines also varies depending on the temperature of the plasma (from the CHIANTI atomic database). The left plot shows the density sensitivity for a range of temperatures with $\log T$ from 5.8 to 6.4. The temperature associated with the maximum formation is $\log T = 6.15$, with the contribution function dropping off steeply toward lower and higher temperatures. The right plot shows the same dependency, but now the ratio is plotted as a function of temperature for a range of densities. The densities in the active region studied vary between $\log n_e = 9$ and 10.

Are the differences between the observed and predicted ratios caused by Lyman continuum absorption in the moss regions of 195 Å emission? Our results hinge on the fact that the observed spatial variation of the 195/1242 Å ratio between moss and loops is larger than predicted by densities determined from the 186/195 Å ratio. We observe a generally much higher contrast and lower values in the map of observed ratios. Several mechanisms could potentially contribute to this mismatch between the predicted and observed ratios. We argue in what follows that none of these can explain our observations and that Lyman continuum absorption is the most likely cause.

A first effect is the temperature dependence of the 195/1242 Å line ratio. This temperature sensitivity was briefly discussed by Del Zanna & Mason (2005) and is illustrated in Figure 4. We see

from the top panel that for the range of densities we observe in this active region ($\log n_e = 9$–10) the 195/1242 Å line ratio can vary from 5 to 3 for $\log T = 5.8$ to from 15 to 10 for $\log T = 6.4$. Both of these temperature values are on the extreme end of what we are most likely observing in these passbands, since the contribution functions of both lines are sharply peaked around $\log T = 6.15$.

We believe that in the coronal loops this temperature dependence can explain some of the spatial variations of the 195/1242 Å line ratio. In loops, we observe these variations to be larger than predicted. However, we argue that in the moss regions, the temperature dependence does not impact our result. We know from the 186/195 Å ratio that the densities in the moss are of the order of $\log n_e = 9.5$–10. In principle, our low observed values of the 195/1242 Å ratio in the moss could thus be caused by a much lower temperature ($\log T = 5.8$), since Figure 4 shows ratios of the order of 3–4. However, we know that moss is always associated with high pressure, hot and dense loops. So, if the upper transition region moss really had a temperature that is much lower than the peak of the Fe XII contribution function, then the high pressure, dense coronal loops that are associated with the upper TR moss would include plasma with temperatures at $\log T = 6.15$. Since the loops associated with moss are high pressure and dense and at the temperature corresponding to the peak of the Fe XII contribution function, these loops would be very bright in the Fe XII rasters. However, we do not observe any such loops in or around the mossy regions. Our observations thus indicate that the temperature of the moss is not low enough to cause the low levels of 195/1242 Å ratios that we observe in the moss. The lack of Fe XII loops connecting to moss has also been observed for other active regions by Antiochos et al. (2003).

Another effect that could contribute to the mismatch between the observed and predicted 195/1242 Å ratio in moss regions is the presence of blends. Any effects of blends can only impact our results and conclusion if the blends preferentially occur in loops or moss. We now show that the effect of blends does not change our results. Young et al. (2009) have studied the density sensitivity of the 186.88 Å and 195 Å lines in detail. They find that there are several uncertainties in the determination of the intensities of the Fe XII 186 and 195 Å lines that can potentially impact our analysis. There is a weak line at 186.98 Å just redward of the Fe XII line, which is likely a Ni XI transition (Young et al. 2009). In our analysis, we avoid contributions of this line by excluding the wavelength range around the Ni XI line in our calculation of the total intensity of the Fe XII 186.88 Å line. The Fe XII 186.88 Å is also impacted by a weak blend of S XI at 186.84 Å (Young et al. 2009). Under equilibrium conditions, this line is formed at $\log T = 6.3$, slightly higher than the $\log T = 6.15$ temperature of the Fe XII line. Young et al. (2009) find that the S XI intensity is typically 2%–5% of the Fe XII 186.88 Å line, which is smaller than the photon noise on the observed Fe XII 186.88 Å intensities. Given the density sensitivity of the 186/195 Å ratio (Figure 1), such a small difference cannot lead to a significant reduction in the discrepancy between predicted and observed 195/1242 Å intensity ratio in the moss regions. To remove the factor of 2 discrepancy in 195/1242 Å ratio would require a change in the 195/186 ratio by a similar factor. Clearly the S XI blend is too weak to impact our results. In addition, even if the blend was much stronger than previously observed, it would more likely impact the hotter moss regions, because the S XI line is formed at slightly higher temperatures. That would mean that in the moss the Fe XII 186.88 Å intensity is overestimated by our analysis, which would lead to a predicted 195/1242 Å intensity ratio with even less difference between moss and loops than is observed.

Young et al. (2009) show that the Fe XII 195.12 Å line similarly has some weak lines in its immediate vicinity. We again avoid contributions of these lines by excluding the wavelength range of these weaker lines in our calculation of the total intensity of the Fe XII line. This line is also blended by another Fe XII line, which is at levels of less than 10% for the densities we find here ($<10^{10}$ cm^{-3}). Given the weakness of the blend, and the fact that the brightness of the blend should not show any difference between moss and loops (since it is also Fe XII), this blend cannot change our conclusions.

Young et al. (2009) have compared densities from different line pairs and found some discrepancies. They suggested that the density determination from the Fe XII 186.88 and 195 Å pair may lead to overestimates of the density by 0.2–0.4 dex, especially in higher density regions. Since our observations show that the moss regions have the highest densities, this currently unexplained effect (most likely due to uncertainties in the atomic data) could lead us to overestimate the moss densities. However, overestimates of the density in moss would lead to even higher values for the predicted ratio of Fe XII 195 and 1242 Å intensity. In summary, this issue would not remove, but rather exacerbate the discrepancy between the observed and predicted ratios.

We have also investigated the effects of the main sources of noise on the EIS spectra. We calculated the errors on our intensities using the `eis_prep` software that is part of the EIS solarsoft tree, and found that photon (Poisson) noise dominates the relative errors. In the moss and loop regions we study, the spectra are high signal-to-noise, of the order of 20 for the 186.88 Å line and 30–40 for the 195 Å line. This means that the relative errors σ on the intensities are small, of the order of 5%. If we assume a worst case scenario in which, e.g., the 186.88 Å intensity is lowered by σ_{186} and the 195 Å intensity is increased by σ_{195}, the predicted 195/1242 ratio map is shifted to higher values. However, such a shift occurs in equal measure for moss and loop regions, so that the predicted spatial variation of the 195/1242 Å ratio cannot be reconciled with the observed ratio. In other words, while these errors can introduce noise on the predicted ratio, they cannot explain the consistently lower values of the 195/1242 ratio that we observe in the moss regions. A similar argument can be made for the absolute calibration errors between SUMER and EIS. Such errors will not depend on the nature of the solar region observed (especially since those are of similar brightness), and cannot explain the spatial variation we observe.

We conclude that the most likely explanation for our EIS/SUMER observations is that EUV emission (at 195 Å) in upper TR moss is reduced in brightness by a factor of the order of 2 because of absorption from neutral hydrogen and helium, and singly ionized helium in the chromospheric jets that permeate the moss.

4. ANALYSIS OF *STEREO* OBSERVATIONS

The region we study with EIS and SUMER was observed by *Hinode* and *SOHO* close to disk center. However, it was also observed by both *STEREO* spacecraft (*SC*). The multiple vantage points these spacecraft provide allow us to also investigate the effect of the angle θ between the line-of-sight vector and the local vertical on the chromospheric absorption of TR EUV emission. We use simultaneous *STEREO A* and *B* images taken

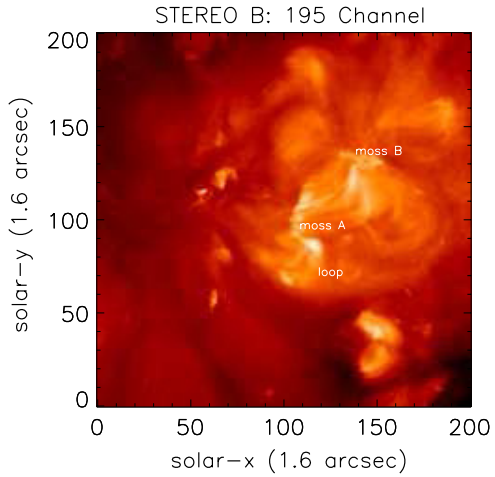

Figure 5. Fe XII Å image of the same active region studied with EIS and SUMER, as seen with *STEREO B*. Marked are three regions of interest (one loop region and two moss regions) for which the intensities seen with *STEREO A* and *B* are compared (see Figure 6). *STEREO A* observed this region at disk center, whereas *STEREO B* observed the region at a viewing angle of 40 deg (with the local vertical).

(A color version of this figure is available in the online journal.)

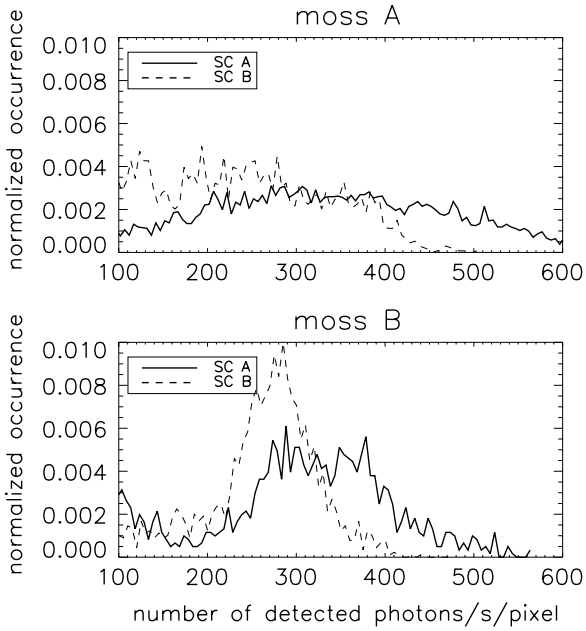

Figure 6. Histograms of the intensity in the two moss regions (marked as A and B in Figure 5) for Fe XII 195 Å observed with *STEREO A* (full line) and *STEREO B* (dashed line). Both regions are reduced in intensity by a factor of roughly 0.75 when viewed with *STEREO B*. This reduction in intensity is caused by Lyman continuum absorption of EUV emission by chromospheric plasma that occurs at similar heights as the EUV emission. Such absorption is increased when the region is viewed from the side, since the observable surface area of chromospheric plasma is increased.

in the Fe XII 195 Å passband of SECCHI on 2007 November 14 during the EIS and SUMER rasters (i.e., between 16 and 18 UTC). The images were corrected for dark current using the software provided in the *STEREO* solarsoft package. To account for the different distance to the Sun of both spacecraft, we correct the intensities observed by *STEREO A* by multiplying the *SC A* intensities with a factor of $(R\mathrm{sun}_A/R\mathrm{sun}_B)^2 = (994/920)^2$, where $R\mathrm{sun}_A$ and $R\mathrm{sun}_B$ is the solar radius in arcseconds as seen from *SC A* and *B*, respectively.

We study the brightness of the three regions of interest in this active region as observed with *SC A* and *B*. Figure 5 shows a *SC B* image of the two moss regions we selected as well as a loop-like structure. All of these regions also occur in the EIS and SUMER rasters of Figure 1. The region is seen at disk center by *STEREO A*, and at an angle of 40 deg between line of sight and local vertical by *STEREO B*. We determine a histogram of intensities seen by *SC A* and *SC B* for the three regions of interest. We find that the average intensity of the loop is the same for *SC A* and *B* (to within 5%). The observed discrepancy is within the range expected from the absolute calibration error, which is estimated to be of order less than 10%.[6] In contrast, the histogram of intensities for both moss regions (Figure 6) shows significant differences, with the emission seen by *SC B* reduced to 75% of that seen by *SC A*. Moss region A shows an average intensity of 340 (normalized units) with a standard deviation of 130 when seen by *SC A*, whereas it is weaker at 240 ± 93 for *SC B*. Similarly, moss region B is at 310 ± 100 for *SC A*, and 260 ± 60 for *SC B*. This is confirmed by the histogram plots, which show a marked increase of very bright features seen with *SC A* (Figure 6).

We find that the coronal loop intensities do not change, whereas the moss region intensities decrease significantly when viewed from the side (at a viewing angle of 40 deg). These results indicate that there is a significant increase of absorption by neutral hydrogen or helium in moss regions when those are viewed from the side. The fact that the loop intensities do not change significantly is to be expected since such loops occur high in the corona, where there is little neutral hydrogen or helium. In contrast, the mix of cool jets and hot plasma in moss regions implies that an observer who views the moss from the side (at a non-negligible viewing angle from the local vertical) will see a larger surface area of chromospheric plasma, which will lead to increased absorption. The amount of absorption seems to roughly scale, perhaps coincidentally, as $\cos\theta$, with $\theta = 40$ deg for our observations.

5. ANALYSIS OF SIMULATIONS

The presence of significant chromospheric absorption of TR EUV emission with wavelengths shorter than 912 Å is confirmed by advanced radiative MHD simulations. In the Oslo Stagger Code (Hansteen et al. 2007) models of the solar atmosphere stretching from the convection zone to corona are constructed. These models include convection, nongray, non-LTE radiative losses in the photosphere, chromosphere, and corona, as well as conduction along the magnetic field.

An initially potential magnetic field is inserted into a fully convective model of dimensions $16 \times 8 \times 15.5$ Mm^3 of which 1.5 Mm is below the photosphere and 14 Mm above. The grid size in the horizontal direction is 65 km, with a smaller grid size of 32 km in the vertical direction. Convective motions and photospheric granular dynamics stress the magnetic field resulting in an upwardly propagating Poynting flux that is dissipated in the outer solar layers. After approximately 20 minutes solar time, and depending on the initial magnetic field strength and topology, the dissipated energy is sufficient to raise and maintain the temperature in the upper layers to coronal values. Thus, a simulated atmospheric structure emerges, with photosphere, chromosphere, and corona much as one believes exists on the Sun. In the present context, we point out that the chromosphere–corona interface, the transition region, in this

[6] J.-P. Wuelser (2008, private communication).

model is extremely corrugated ranging in height from some 1.5 Mm to 5–6 Mm above the photosphere. Thus, at any given time we find plasma at temperatures ranging from 5000 K to 1 MK in the same height range. As a consequence cool plasma in sufficient quantities to absorb short wavelength EUV radiation is found at these heights.

To quantify this we calculate the intensity in both the Fe XII 1242 Å and 195 Å lines from a given snapshot. This is accomplished by integrating the optically thin contribution function

$$dI = A_{\rm el} n_{\rm e}^2 g(T) e^{-\tau} dz$$

along rays parallel to the "line of sight," where $A_{\rm el}$ is the element abundance relative to hydrogen, $n_{\rm e}$ is the electron density, τ is the optical depth of the absorbing opacity, and $g(T)$ is a function that incorporates the ionization state of the radiating material and the collisional excitation rates:

$$g(T) = 0.83 h\nu n_j A_{ji} f(T)/n_{\rm e}.$$

Here, $h\nu$ is the energy of the transition, n_j is the population of the upper level of the radiating ion, A_{ji} the Einstein coefficient for the transition, and $f(T)$ the ionization state of the radiating ion (Dere et al. 1997; Landi et al. 2006). The optical depth τ is computed assuming that all absorption comes from neutral hydrogen and neutral and singly ionized helium such that following Anzer & Heinzel (2005) we write

$$\tau = \sigma_{\rm H\,I} N_{\rm H\,I} + \sigma_{\rm He\,I} N_{\rm He\,II} + \sigma_{\rm He\,II} N_{\rm He\,II},$$

where $N_{\rm H\,I}$ is the total column density of neutral hydrogen along the line of sight, and $N_{\rm He\,I}$ and $N_{\rm He\,II}$ are those of neutral and singly ionized helium. The σ-values are the respective photoionization cross sections which depend only on wavelength. In computing the column densities of hydrogen and helium we assume the ionization derived by Mazzotta et al. (1998) as found in the CHIANTI package.

In Figure 7, we plot the emergent intensities of the Fe XII 1242 Å and 195 Å lines as seen from the side, e.g., as seen at the limb. Note the significant differences between the intensities, both in the higher-lying loops (because of density sensitivity), and at the lower regions near the footpoints of the loops ($z < 3$ Mm) because of the chromospheric absorption of EUV photons that have wavelengths below 912 Å. The presence of almost complete extinction of the 195 Å intensity in the lower 1–3 Mm of the coronal loops is caused by absorption from upper chromospheric extrusions into coronal territory.

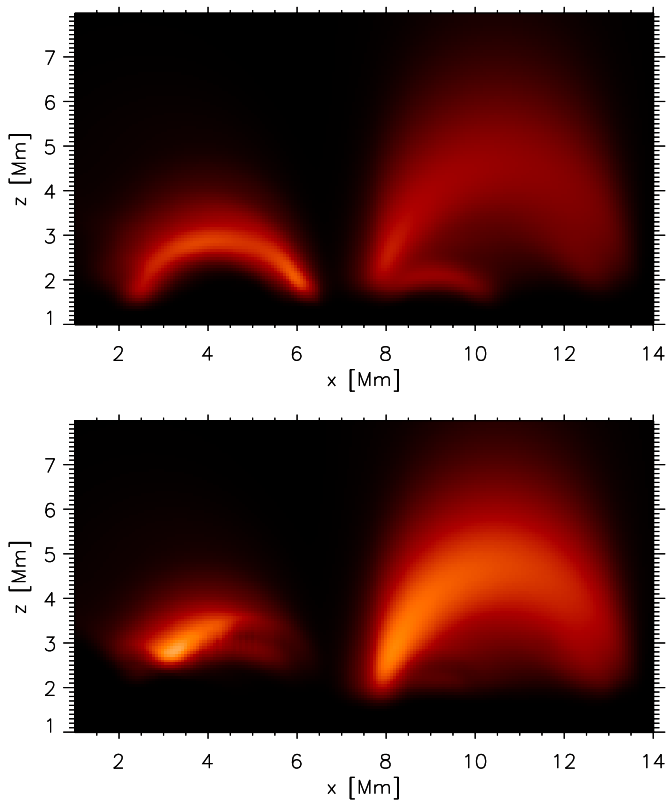

Figure 7. Side views of synthetic Fe XII intensities from our 3D radiative MHD simulation. The intensity shown in each panel is summed along a ray parallel to the *y*-axis (perpendicular to the plane of the figure) using the density and temperature in the simulated box, and CHIANTI to calculate the emergent intensity. The top panel shows Fe XII 1242 Å emission, whereas the bottom panel shows Fe XII 195 Å emission. Note the significant differences between the intensities, both in the higher-lying loops (because of density sensitivity), and at the lower regions or footpoints of the loops ($z < 3$ Mm) because of the absorption of EUV photons that have wavelengths below 912 Å. See the text for details.

(A color version of this figure is available in the online journal.)

6. SUMMARY

We find evidence for significant absorption of EUV emission (with wavelengths below 912 Å) in the transition region of coronal loops because of the presence at similar heights of dense, chromospheric gas. We use the Fe XII 186.88, 195, and 1242 Å lines from quasi-simultaneous *Hinode*/EIS and *SOHO*/SUMER spectra of an active region and show that the transition region emission in moss regions is reduced by a factor of the order of 2 because of absorption by neutral hydrogen and helium and singly ionized helium that occurs at similar heights in chromospheric jets. We use *STEREO*/SECCHI observations of the same active region using both spacecrafts and find that this absorption is further increased when moss regions are viewed closer to the limb. These observational results are confirmed by advanced three-dimensional (3D) numerical simulations which show similar levels of absorption because of comingling of cool, chromospheric plasma and hot, upper transition region plasma at similar heights.

The determination of this type of absorption significantly reduces or removes an uncertainty that has plagued comparisons of EUV images with numerical models of coronal loops, which have had trouble reconciling the observed and predicted EUV brightness at the footpoints of loops. Current models typically show a mismatch of 1 order of magnitude. A variety of attempts at reducing the discrepancy include height (and magnetic field) dependent filling factors, time-dependent heating models, etc. By determining what the real, unobstructed emission in the upper transition region of coronal loops is, our results reduce (but do not totally remove) the current discrepancy and will guide modelers toward better constraints on their free parameters and assumptions. The *STEREO* observations and numerical results suggest that full Sun models need to also consider the center-to-limb variation of the absorption.

The significant absorption of EUV emission in the transition region by cool plasma in chromospheric jets indicates that coronal loop modelers should be aware of and take into account the properties of the absorbing jets. For example, is it possible that the observed inverse correlation between "filling factor" and coronal loop pressure reported by Warren et al. (2008) is related to the dependence on coronal pressure of the height range

over which the transition region occurs in combination with the presence of absorbing jets? Given the significant absorption by chromospheric jets, more attention is also warranted for the effects of chromospheric absorption on the detailed shape of line profiles of coronal emission lines (see, e.g., Spadaro et al. 1996).

The total amount of absorption we find is of the order of at least 2–3 (for viewing angles of less than 40 deg from disk center). Further observations with *STEREO*/SECCHI for a wider variety of viewing angles have the potential of revealing the true center to limb variation of moss brightness, which can be compared to that of numerical simulations, and may reveal details about the filling factor and orientation of chromospheric features in the moss phenomenon. In addition, simultaneous observations with EIS and SUMER of a larger statistical sample of active regions will help determine the variability of this absorption across active regions of varying activity.

S.W.M. acknowledges support from NSF grant ATM-0541567 and NASA grants NNG06GC89G and NNX08AH45G. B.D.P. is supported by NASA grants NAS5-38099 (*TRACE*), NNM07AA01C (*HINODE*), NNG06GG79G, and NNX08AH4 5G. We thank Amy Winebarger and Peter Young for helpful discussions. *Hinode* is a Japanese mission developed and launched by ISAS/JAXA, with NAOJ as a domestic partner and NASA and STFC (UK) as international partners. The SECCHI data were produced by an international consortium of the Naval Research Laboratory (USA), Lockheed Martin Solar and Astrophysics Lab (USA), NASA Goddard Space Flight Center (USA), Rutherford Appleton Laboratory (UK), University of Birmingham (UK), Max-Planck-Institut for Solar System Research (Germany), Centre Spatiale de Liège (Belgium), Institut d'Optique Théorique et Appliqueé (France), and Institut d'Astrophysique Spatiale (France).

REFERENCES

Antiochos, S. K., Karpen, J. T., DeLuca, E. E., Golub, L., & Hamilton, P. 2003, ApJ, 590, 547
Anzer, U., & Heinzel, P. 2005, ApJ, 622, 714
Aschwanden, M. J., Winebarger, A., Tsiklauri, D., & Peter, H. 2007, ApJ, 659, 1673
Berger, T. E., De Pontieu, B., Fletcher, L., Schrijver, C. J., Tarbell, T. D., & Title, A. M. 1999a, Sol. Phys., 190, 409
Berger, T. E., De Pontieu, B., Schrijver, C. J., & Title, A. M. 1999b, ApJ, 519, L97
Culhane, J. L., et al. 2007, Sol. Phys., 243, 19
Daw, A., Deluca, E. E., & Golub, L. 1995, ApJ, 453, 929
De Pontieu, B., Berger, T. E., Schrijver, C. J., & Title, A. M. 1999, Sol. Phys., 190, 419
De Pontieu, B., & Erdélyi, R. 2006, R. Soc. Lond. Phil. Trans. Ser. A, 364, 383
De Pontieu, B., Erdélyi, R., & de Wijn, A. G. 2003a, ApJ, 595, L63
De Pontieu, B., Erdélyi, R., & James, S. P. 2004, Nature, 430, 536
De Pontieu, B., Hansteen, V. H., Rouppe van der Voort, L., van Noort, M., & Carlsson, M. 2007a, ApJ, 655, 624
De Pontieu, B., Tarbell, T., & Erdélyi, R. 2003b, ApJ, 590, 502
De Pontieu, B., et al. 2007b, PASJ, 59, 655
Del Zanna, G., & Mason, H. E. 2005, A&A, 433, 731
Dere, K. P., Landi, E., Mason, H. E., Monsignori Fossi, B. C., & Young, P. R. 1997, A&AS, 125, 149
Domingo, V., Fleck, B., & Poland, A. I. 1995, Sol. Phys., 162, 1
Doschek, G. A., & Feldman, U. 1982, ApJ, 254, 371
Fletcher, L., & De Pontieu, B. 1999, ApJ, 520, L135
Hansteen, V. H., Carlsson, M., & Gudiksen, B. 2007, in ASP Conf. Ser. 368, The Physics of Chromospheric Plasmas, ed. P. Heinzel, I. Dorotovič, & R. J. Rutten (San Francisco, CA: ASP), 107
Hansteen, V. H., De Pontieu, B., Rouppe van der Voort, L., van Noort, M., & Carlsson, M. 2006, ApJ, 647, L73
Heggland, L., De Pontieu, B., & Hansteen, V. H. 2007, ApJ, 666, 1277
Howard, R. A., et al. 2008, Space Sci. Rev., 136, 67
Judge, P. G., Woods, T. N., Brekke, P., & Rottman, G. J. 1995, ApJ, 455, L85
Kaiser, M. L., Kucera, T. A., Davila, J. M., St. Cyr, O. C., Guhathakurta, M., & Christian, E. 2008, Space Sci. Rev., 136, 5
Keenan, F. P., Tayal, S. S., & Henry, R. J. W. 1990, Sol. Phys., 125, 61
Klimchuk, J. A. 2006, Sol. Phys., 234, 41
Kosugi, T., et al. 2007, Sol. Phys., 243, 3
Landi, E., Del Zanna, G., Young, P. R., Dere, K. P., Mason, H. E., & Landini, M. 2006, ApJS, 162, 261
Mariska, J. T. 1992, The Solar Transition Region (Cambridge: Cambridge Univ. Press)
Martens, P. C. H., Kankelborg, C. C., & Berger, T. E. 2000, ApJ, 537, 471
Mazzotta, P., Mazzitelli, G., Colafrancesco, S., & Vittorio, N. 1998, A&AS, 133, 403
McIntosh, S. W., Davey, A. R., Hassler, D. M., Armstrong, J. D., Curdt, W., Wilhelm, K., & Lin, G. 2007, ApJ, 654, 650
Patsourakos, S., & Klimchuk, J. A. 2008, ApJ, 689, 1406
Rouppe van der Voort, L. H. M., De Pontieu, B., Hansteen, V. H., Carlsson, M., & van Noort, M. 2007, ApJ, 660, L169
Rutten, R. J. 2006, in ASP Conf. Ser. 354, Solar MHD Theory and Observations: A High Spatial Resolution Perspective, ed. J. Leibacher, R. F. Stein, & H. Uitenbroek (San Francisco, CA: ASP), 276
Schmahl, E. J., & Orrall, F. Q. 1979, ApJ, 231, L41
Schrijver, C. J., Sandman, A. W., Aschwanden, M. J., & DeRosa, M. L. 2004, ApJ, 615, 512
Spadaro, D., Lanza, A. F., & Antiochos, S. K. 1996, ApJ, 462, 1011
Warren, H. P., & Winebarger, A. R. 2006, ApJ, 645, 711
Warren, H. P., Winebarger, A. R., Mariska, J. T., Doschek, G. A., & Hara, H. 2008, ApJ, 677, 1395
Wilhelm, K., et al. 1995, Sol. Phys., 162, 189
Winebarger, A. R., Warren, H. P., & Falconer, D. A. 2008, ApJ, 676, 672
Young, P. R., Watanabe, T., Hara, H., & Mariska, J. T. 2009, A&A, 495, 587